Supplement of Atmos. Chem. Phys., 25, 13711–13727, 2025 https://doi.org/10.5194/acp-25-13711-2025-supplement © Author(s) 2025. CC BY 4.0 License.





Supplement of

Measurement report: Molecular insights into organic aerosol sources and formation at a regional background site in South China

Hongxing Jiang et al.

Correspondence to: Hai Guo (hai.guo@polyu.edu.hk)

The copyright of individual parts of the supplement might differ from the article licence.

1	
2	
3	
4	
5	
6	The convergent of individual parts of the supplement might differ from the article licenses
O	The copyright of individual parts of the supplement might differ from the article licence
7	

Supplementary text

8

9

HR-TOF-AMS analysis

10 We conducted a comprehensive sampling campaign in autumn 2020 (September 29 to November 18), 11 during the COVID-19 lockdown, at Hok Tsui, a regional background site in Hong Kong, to study the 12 influence of transport from mainland China on local air quality. During this period, we employed an online 13 high-resolution time-of-flight aerosol mass spectrometer (HR-TOF-AMS, Aerodyne Inc.) to measure the 14 chemical composition of NR-PM₁, including total organics, sulfate, nitrate, ammonium, and chloride. The 15 AMS alternated between V-mode and W-mode on a 2-minute cycle. Elemental composition of organics was 16 determined using W-mode data, which provides high mass resolution (~5000-6000), and was subsequently 17 used for OA source apportionment. To ensure the accuracy of NR-PM₁ measurements, the instruments were 18 regularly calibrated with pure chemical standards, such as ammonium nitrate, both before and during the 19 sampling period. Pure ammonium nitrate particles (350nm in diameter) were applied to calibrate the 20 ionization efficiency (IE) for m/z 30 and m/z 46. Based on weekly calibrations, the relative ionization 21 efficiency (RIE) value for ammonium was determined to be 4.0. In addition, particle velocity during 22 sampling was calibrated using Nanosphere PSL particles of various sizes (50, 100, 200, 300, 400, 500, and 23 600nm; Duke Scientific, Palo Alto, CA, USA). The collection efficiency (CE) of NR-PM₁ was determined 24 by comparing AMS NR-PM1 measurements with PM1 concentrations measured by HKEPD, after 25 subtracting black carbon at the same location. PM1 and black carbon concentrations from HKEPD were 26 obtained using a Tapered Element Oscillating Microbalance (TEOM) and a black carbon analyzer (BC, 27 model AE16, Magee, USA), respectively. The final CE value for this study was determined to be 0.73 and 28 was applied to all measured NR-PM₁ components. Finally, the collection efficiency (CE) for this study was 29 determined to be 0.73 and was applied to all measured NR-PM₁ components. 30 Data processing was performed using the ToF-AMS Analysis Toolkit 1.59D and TofAMS HR Analysis 31 1.19D, both implemented in Igor Pro 6.37 software. RIEs of 1.4, 1.1, 1.2, 4.0, and 1.3 were applied for total 32 organics, nitrate, sulfate, ammonium and chloride, respectively. Method detection limits (MDLs) for each 33 species were determined by collecting background mass spectra (HEPA filtered air, 60 min every 2 days). 34 The calculated MDLs wer 0.21 µg m⁻³ for organics, 0.020 µg m⁻³ for nitrate, 0.022µg m⁻³ for sulfate, 0.013 35 μg m⁻³ for ammonium, and 0.013 μg m⁻³ for chloride. OA source apportionment was conducted using the 36 Positive Matrix Factorization (PMF) Evaluation Toolkit (PET v2.05). To ensure robust results, several 37 steps were followed as described in our previous studies, including the application of minimum error values 38 and ion filtration (Huo et al., 2024a; Yao et al., 2022). The optimal 4-factor solution was selected based on 39 Q/Q_{exp} values, residuals, and mass spectra (Zhang et al., 2011). Figure S1 presents the mass spectra of the 4 40 OA factors resolved by PMF. The HOA factor was characterized by abundant alkyl fragments ($C_nH_{2n+1}^+$ and 41 $C_nH_{2n-1}^+$), such as $C_3H_5^+$, $C_3H_7^+$, $C_4H_7^+$, and $C_4H_9^+$ (Sun et al., 2011). In this study, the HOA factor had O/C 42 and H/C values of 0.25 and 1.72, respectively, the lowest and highest among the 4 factors. Notably, the O/C 43 value was higher than typical ranges for HOA reported in previous studies (e.g., 0.05-0.25), indicating the

- influence of atmospheric aging (Huo et al., 2024a). The other 3 factors exhibited high loadings of
- oxygenated species, such as m/z 44 (mainly CO₂⁺), confirming their classification as oxygenated OA
- 46 components. These 3 OOA factors were divided into two less oxidized OOAs (LO-OOA1 and LO-OOA2)
- 47 and one more oxidized OOA (MO-OOA) based on their O/C values. The LO-OOA factors also contained
- 48 many alkyl fragments, indicating a closer association with primary sources.

TAG-EI-TOF-MS analysis

49

67

77

- During the sampling period, TAG-EI-TOF-AMS analysis was used to quantify SOA tracers in the particle
- 51 phase. Detailed descriptions of the instrument and its performance are available in our previous studies
- 52 (Huo et al., 2024b; Lyu et al., 2020). Briefly, air samples were collected using a collection and thermal
- desorption (CTD) unit at 30 °C with a flow rate of 10 L min⁻¹ over 90 min. Derivatization occurred in the
- 54 CTD unit by purging it with a mixed flow of pure helium (20 mL/min) and saturated N-methyl-N-
- 55 (trimethylsilyl) trifluoroacetamide (MSTFA)-helium (80 mL/min). The CTD unit was heated to 315 °C
- over 9 minutes and held at that temperature for 5 minutes, allowing derivatives to be desorbed and
- 57 transferred to a focusing trap (FT) unit (~30 °C), where target compounds and their derivatives were
- trapped while excess MSTFA and most volatile organics were vented. The FT was then gradually heated to
- 59 315 °C over 12 minutes, with pure helium purging the target compounds from the FT to a mini-gas
- 60 chromatography (GC) column. The GC column was operated under a programmed temperature profile
- 61 (0.75 mL/min), starting at ~40 °C and increasing to 45 °C in 1 minute, then rapidly rising to 330 °C over 10
- 62 minutes, and held at 330 °C for 12 minutes until the end of the GC analysis. Before sampling, external
- standards with known concentrations were used for identification and quantification of target compounds.
- To address desensitization and peak drift during analysis, a mixture of 26 deuterated internal compounds
- with constant concentrations was injected alongside each sample. In total 62 compounds were identified,
- with details provided in Table S2.

PTR-TOF-MS analysis

- An online proton transfer reaction quadrupole ion time-of-flight mass spectrometer (PTR-TOF-MS,
- 69 IONICON Analytik GmbH, Innsbruck, Austria) was used to measure concentrations of VOC species.
- 70 Detailed information about the instrument is available in previous studies (Yuan et al., 2024). Ambient air
- 71 was continuously drawn at a rate of 3.0 L/min through a Teflon tube equipped with a 4.7 mm Teflon-
- membrane filter (Whatman Ihc. Clifton, NJ, USA). A small fraction of this air (0.2 L/min) was introduced
- 73 into the TOF-MS for VOCs measurements. Certified standard gas mixtures (1 ppm, Linde Spectra
- Environmental Gases, USA) were used to quantify target VOCs species, determine the instrument's
- 75 transmission curve, and assess sensitivities. The PTR-TOF-MS was calibrated weekly at room temperature
- vsing a liquid calibration unit (LCU, Ionicon).

Other ancillary measurements

- In addition to the online instruments used for detecting atmospheric organics, a suite of other online
- instruments was employed to measure concentrations of PM_{2.5}, trace gases (CO, NO, NO₂, O₃ and SO₂), and
- 80 meteorological parameters (temperature and relative humidity). PM_{2.5} concentrations were measured using
- a Tapered Element Oscillating Microbalance (TEOM) (Thermo ScientificTM 1405). SO₂ concentrations
- 82 were determined with a Teledyne Advanced Pollution Instrumentation (API) Trace-level UV Fluorescence
- 83 SO₂ Analyzer (T100U), while nitrogen species were measured using the Teledyne True NO₂/NO/NO_x
- Analyzer (T200UP) Ozone (O₃) concentrations were measured With an Ecotech UV Absorption Ozone
- Analyzer (EC9810B/S10). The photolysis frequency of NO₂ (jNO₂) was measured using a MetCon Filter
- 86 Radiometer.

95

Carbon analysis

- The concentrations of organic carbon (OC) and elemental carbon (EC) in PM_{2.5} were determined using a
- 89 Sunset OC/EC analyzer with an enhanced thermal/optical reflectance protocol. A 1.5 cm² section of each
- 90 PM_{2.5} filter was placed in a quartz boat and subjected to stepwise heating in a quartz furnace to separate OC
- and EC. During analysis, four OC peaks (OC1, OC2, OC3, and OC4) and three EC peaks (EC1, EC2, and
- 92 EC3) were identified. Pyrolyzed organic carbon (PyC), formed by the coking of OC during the procedure,
- 93 was monitored through changes in laser reflectance signals. The total OC and EC contents were calculated
- using the formulas as follows: OC = OC1 + OC2 + OC3 + OC4 + PyC; EC = EC1 + EC2 + EC3 PyC.

HR-orbitrap-MS analysis

- The molecular composition of OAs in offline PM_{2.5} filters was analyzed using a high-resolution Q-
- 97 Executive Orbitrap mass spectrometer (Thermo Electron, Inc.) coupled with an ultra-high performance
- 98 liquid chromatography system (UHPLC, Dionex UltiMate 3,000, Thermo Electron, Inc.). Detailed
- descriptions of the analysis procedures and instrumental settings are available in a previous study (Zhang et
- al., 2024). Briefly, two pieces of PM_{2.5} filters were punched using a stainless-steel puncher (Φ=20 mm), and
- the dissolved organic matter was extracted with 6 mL of mix-solvents (2×3 times, methanol: toluene=1:1,
- v/v) in an ultrasonic cold-water bath for 20 minutes. The extracts were filtered through a 0.22 μ m
- polytetrafluoroethylene filter membrane, combined, and evaporated to near dryness under a gentle stream
- 104 of high-purity nitrogen. The residue was then redissolved in 150 μL of methanol and centrifuged, with the
- supernatant transferred for subsequent HR-MS analysis.
- As noted in previous studies, potential intermolecular suppression effects can occur during the ionization
- process (Zhang et al., 2024; Thoma et al., 2022). To address these challenges, a UHPLC system was
- 108 employed for compound separation. Samples (5 μL) were injected into the system, and separation was
- performed on an Acquity UPLC HSS T3 column (1.8 µm particle size, 100 mm × 2.1 mm; Waters, Milford,
- MA, USA) with a VanGuard pre-column (HSS T3, 1.8 μm) at a flow rate of 0.3 mL min⁻¹. A gradient
- elution procedure was used for compounds isolation, with eluent A/B consisting of 0.1% formic acid in
- 112 ultrapure water/methanol. Eluent B was initially maintained at 10% for 2 min, increased to 54% over 15.2

min and held for 1 min, then increased to 90% over 7.5 min and held for 0.2 min, before returning to 1% within 1.8 min and held for 9.6 min before the next sample. Analytes were introduced to the heated electrospray ionization (ESI) source system and ionized in negative mode. The spray voltages were set as 3.0 kV for ESI–, with the capillary temperature at 320°C. The sheath gas flow, auxiliary gas flow, and

sweep gas flow were set 35, 10, and 0 units, respectively. The mass spectrometer scanned a range of m/z

118 50-800 with a typical mass resolution of 140,000 at m/z 200.

Xcalibur software (V2.2; Thermo Scientific) was used to acquire raw data, while further non-target
 compound analysis was performed using the open-source MZmine-2.37 software (http://mzmine.github.io).
 This analysis included raw data import, peak detection, shoulder peak filtering, chromatogram building,
 chromatogram deconvolution, deisotoping, searching for adducts and peak complexes, alignment, gap

chromatogram deconvolution, deisotoping, searching for adducts and peak complexes, alignment, gap filling, identification, and duplicate peak filtering. Detailed processing steps and settings are described in

previous literature (Wang et al., 2017). Mass peaks were assigned to specific molecules with a mass

125 tolerance of 2 ppm for ESI- mode. The atoms in the assigned molecular formulas were limited to

 $126 \qquad C_{1-40}H_{0-100}O_{0-40}N_{0-5}S_{0-3}, \ with \ additional \ criteria \ on \ elemental \ ratios \ (e.g., \ H/C, \ O/C) \ and \ double \ bond$

equivalents (DBE) applied to eliminate chemically meaningless molecular formulas. The elemental ratios,

DBE, and modified aromatic index were calculated based on the assigned formulas of $C_cH_hO_oN_nS_s$, where

c, h, o, n, and s represent the number of carbon, hydrogen, oxygen, nitrogen, and sulfur atoms, respectively.

All molecules reported in this study underwent blank subtraction, and those with an abundance ratio of less

than 5:1 were eliminated (Ditto et al., 2018).

The chemical parameters, including DBE, nO_{eff} , (Nie et al., 2022), AI_{mod} (Koch and Dittmar, 2006), and

volatility (LogC*) (Li et al., 2016), of the compounds are calculated using the following equations

134 respectively:

123

130

DBE =
$$(2 n_C + 2 - n_H + n_N)/2$$

$$nO_{eff} = n_O - 2 n_N - 3 n_S$$

$$AI = (1 + n_C - 0.5 n_O - n_S - 0.5 n_H) / (n_C - 0.5 n_O - n_S - n_N)$$

$$Log_{10}C^* = (n_C^0 - n_C)b_C - n_Ob_O - 2\frac{n_C n_O}{n_C + n_O}b_{CO} - n_N b_N - n_S b_S$$

where n_C , n_H , n_O , n_N , and n_S denote the numbers of carbon, hydrogen, oxygen, nitrogen, and sulfur atoms in the molecular formula, respectively. n_C^0 is the reference carbon number. The parameters b_C , b_O , b_N , and

 b_S denote the contribution of each atom to $log_{10}C^*$, respectively, while b_{CO} is the carbon-oxygen

142 nonideality.

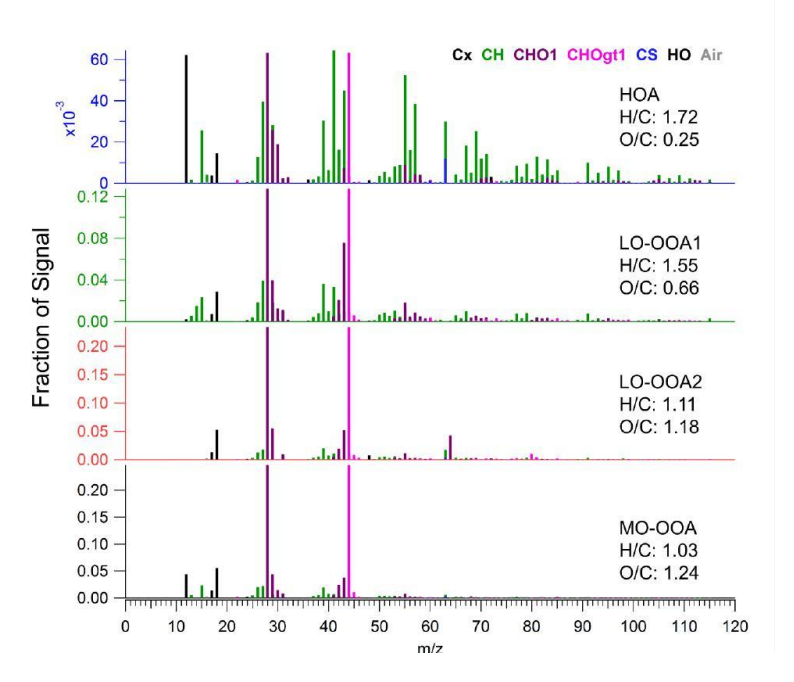


Figure S1. Mass spectra of OA components obtained from AMS-PMF analysis

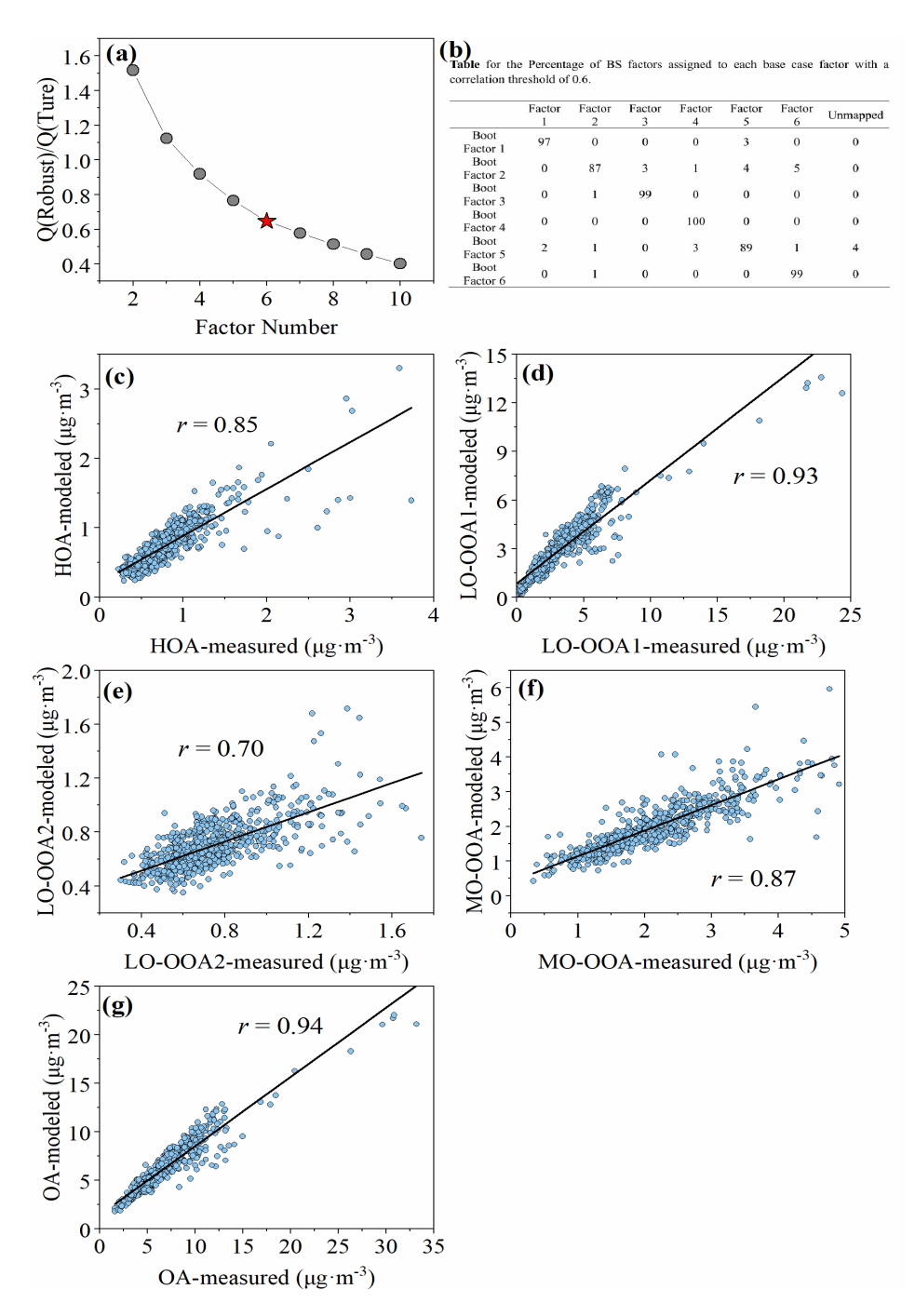


Figure S2. Diagnostic results for tracer-based PMF analysis. (a) Variation of average Q/Q_{exp} with increasing number of factors in PMF. (b) Table showing the percentage of bootstrap (BS) factors assigned to each base case factor, using a correlation threshold of 0.6. (c-g) Correlation analysis between the concentrations of AMS-PMF derived OA components and the tracer-based PMF modeled values

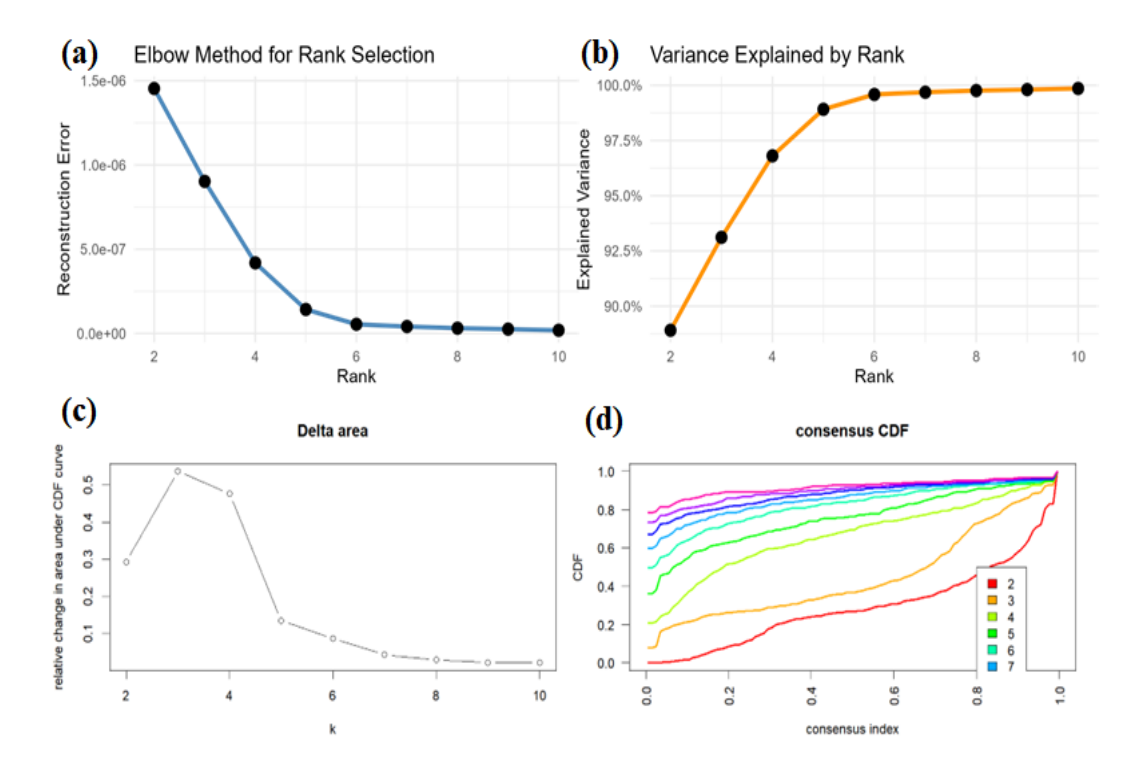


Figure S3. Diagnostic results for PMF results-constrained NMF analysis. (a) Variation of re-constructured error with increasing number of factorss. (b) Variation of explained total variances with increasing number of factors. and (c) Variation of the cumulative distribution function (CDF) delta area with increasing number of factors. (d) Cumulative distribution functions of the consensus matrix for each factor number, estimated using a histogram with 100 bins

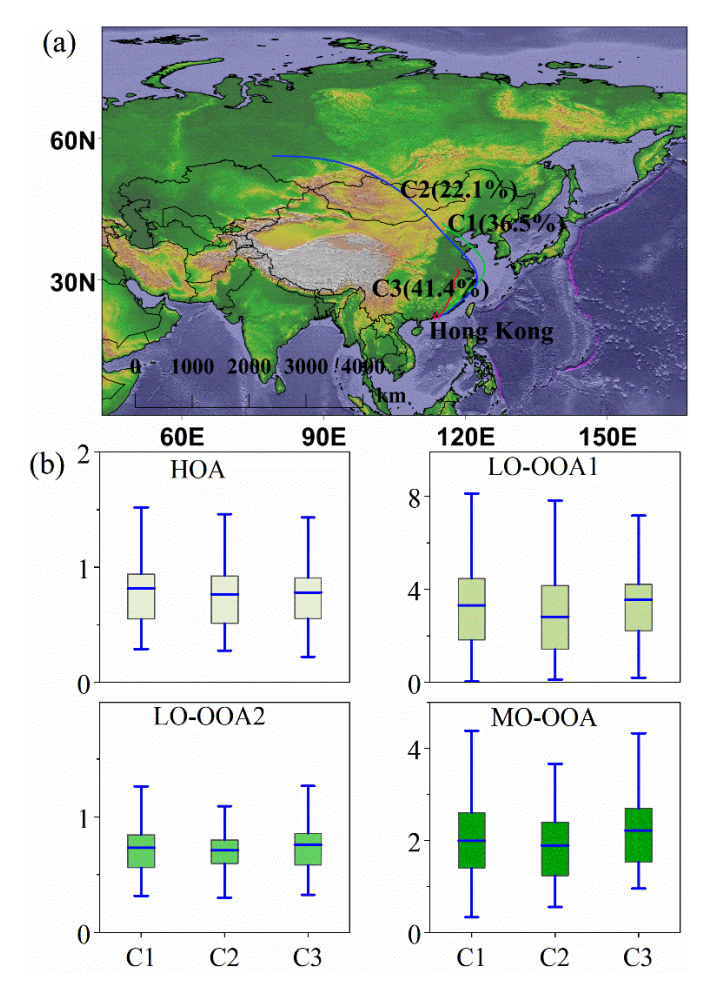
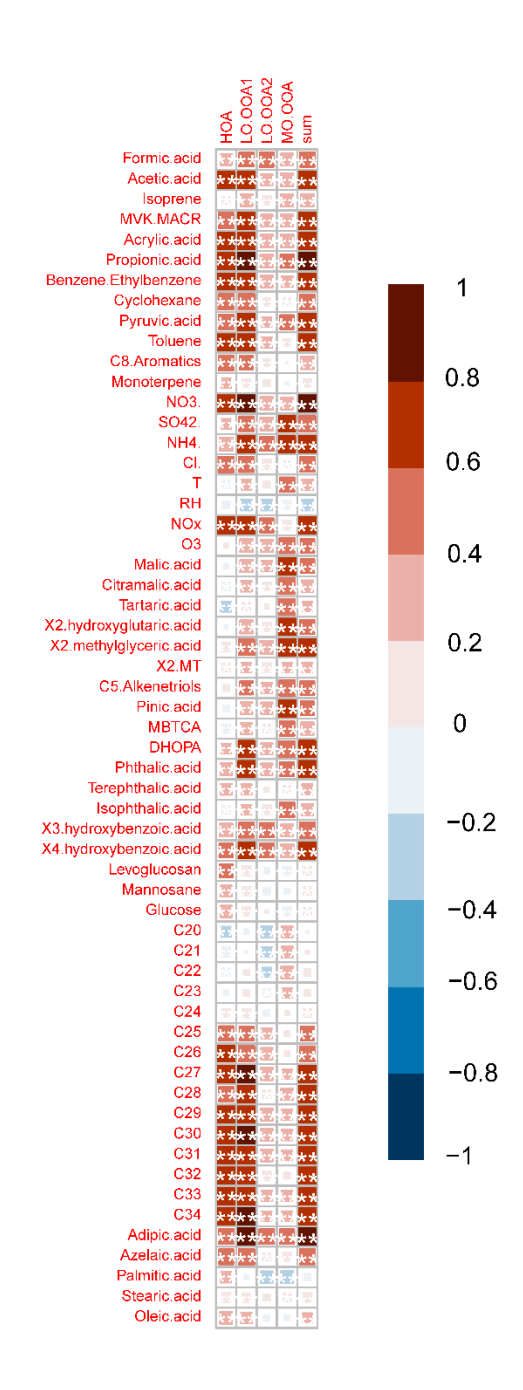


Figure S4. (a) Air mass clusters based on 120 - hr backward trajectories arriving at the sampling site during the study period. (b) Box plots of the four OA components for different air mass influence periods. In each box, the blue line denotes the mean value, the upper (lower) boundary of the box represents the 75th (25th) percentile, and the top and bottom whiskers indicate the 95th and 5th percentiles, respectively.



163 Figure S5. Correlations between AMS-PMF derived OA components and selected chemical species.

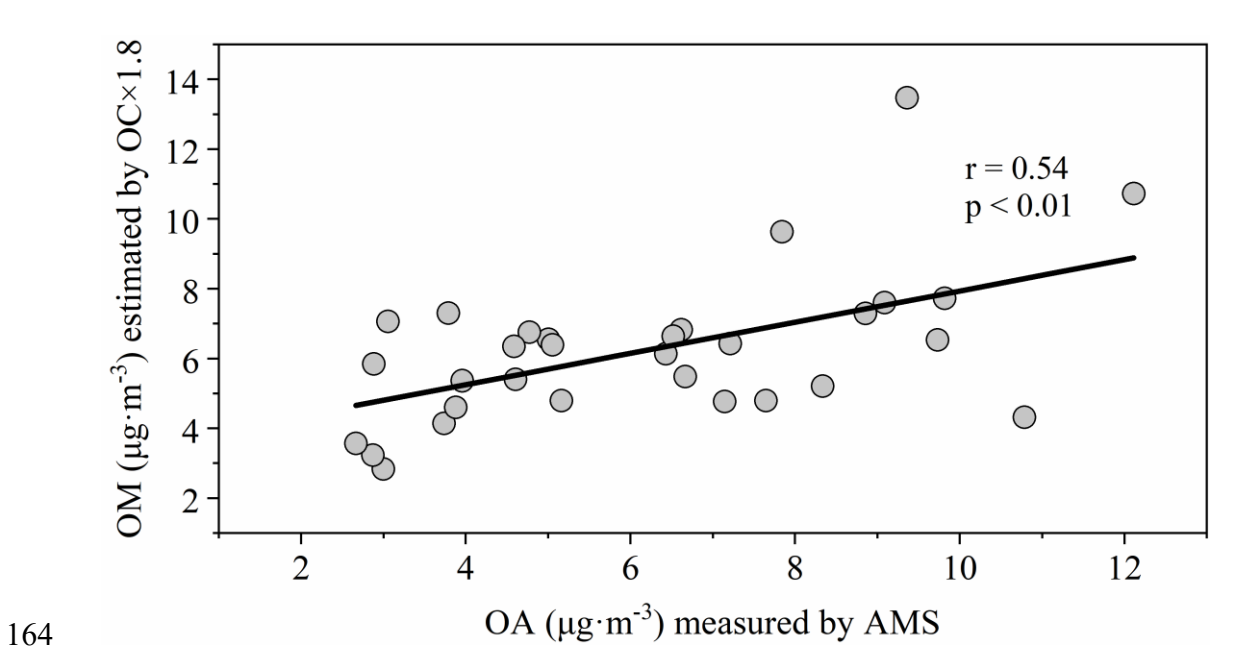


Figure S6. Correlations between AMS-derived OA concentrations and estimated OM (OC multiplied by a factor of 1.8). The observed correlation coefficient suggests that, despite uncertainties in OM estimation, potential discrepancies between AMS and OC/EC analyzer measurements, and the limited sample size, OA in PM₁ likely shares similar sources and formation pathways with OM in PM_{2.5}.

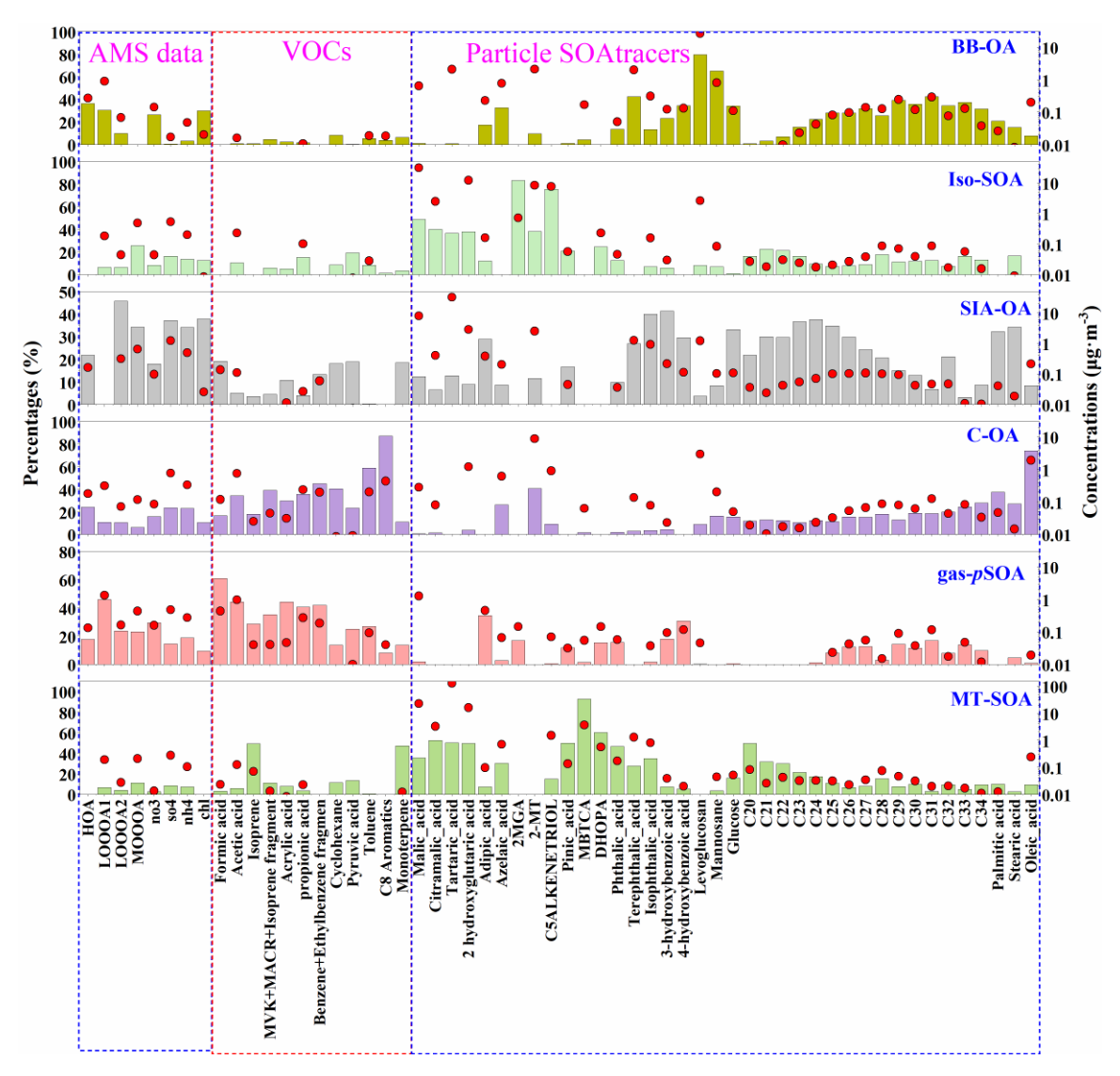


Figure S7. Source profiles of individual factors identified in the 6-factor solution resolved by tracer-based PMF.

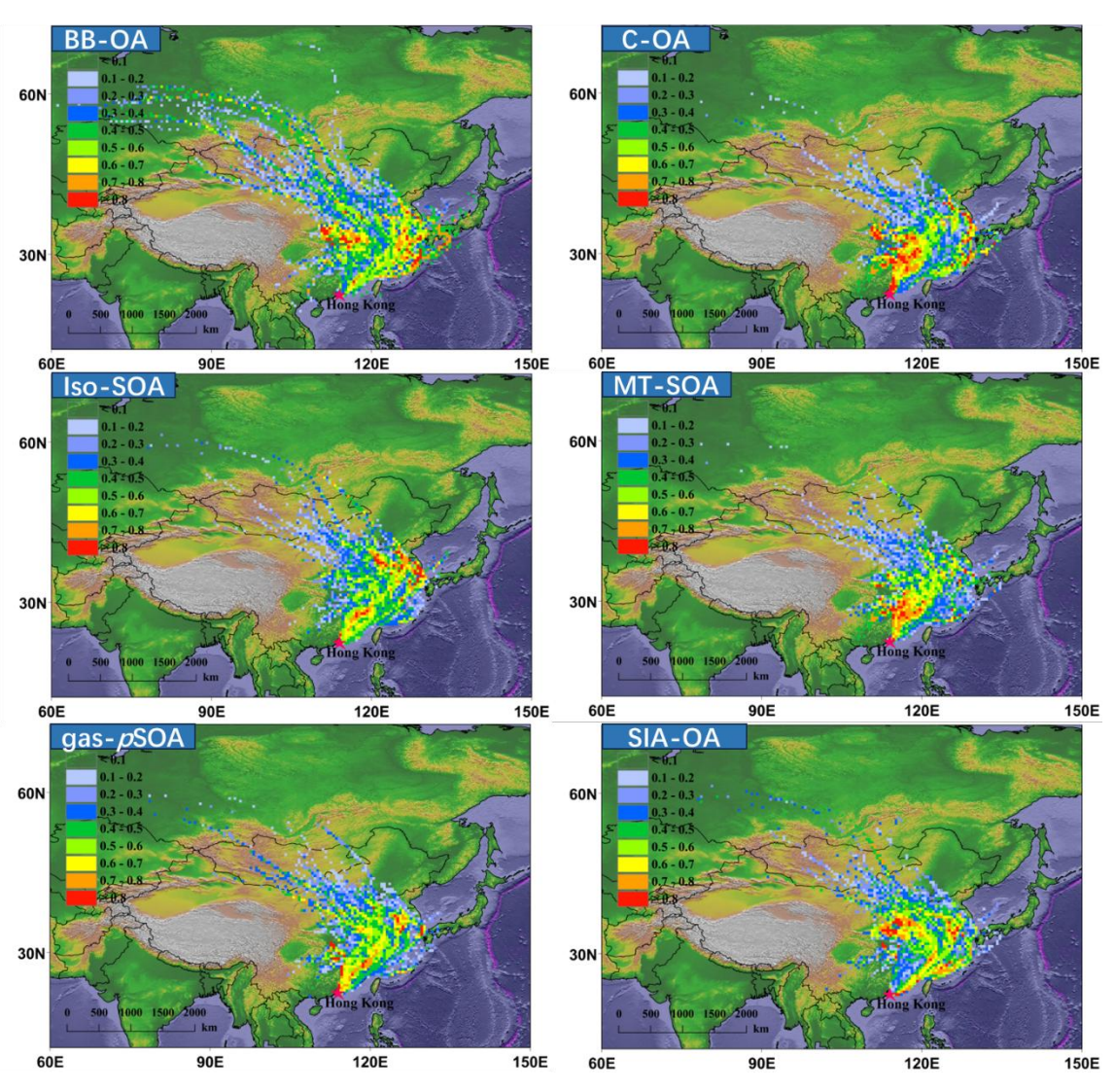


Figure S8. PSCF maps of the 6 PMF-resolved sources during the sampling period. The color gradient denotes the potential source contributions.

173

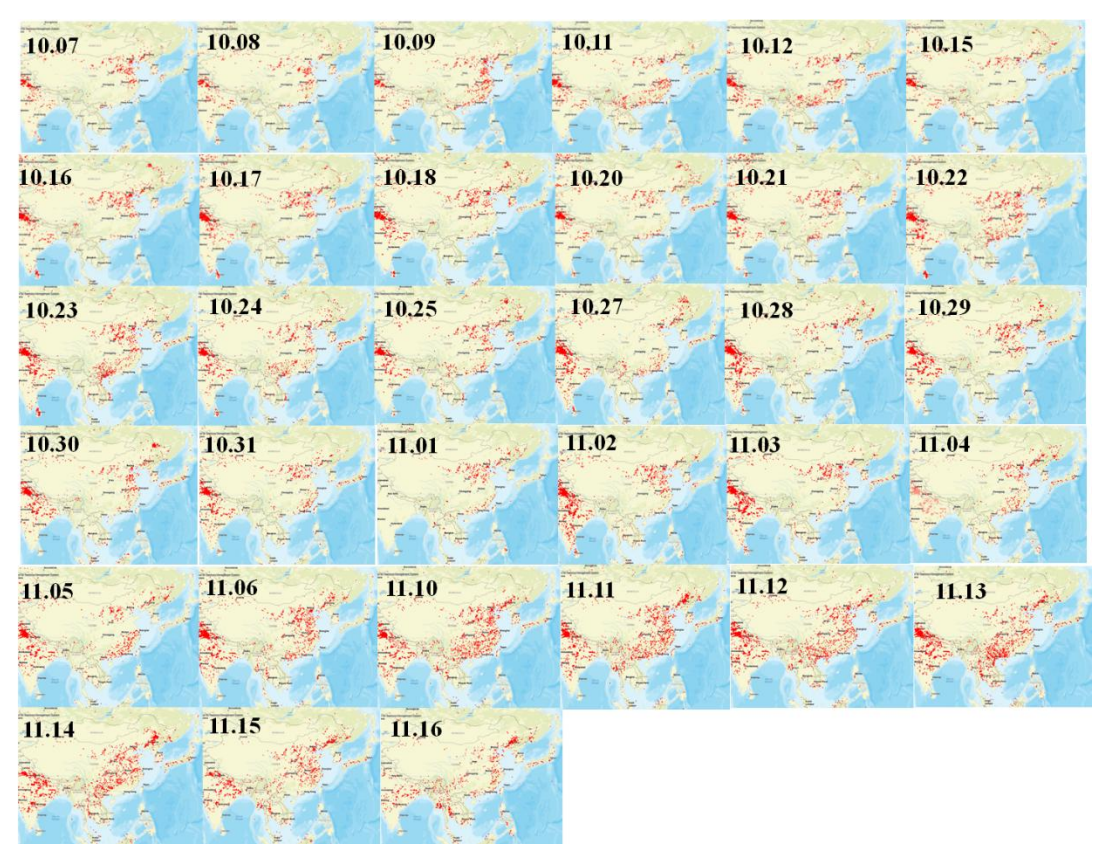


Figure S9. Daily fire maps corresponding to the offline PM_{2.5} filter sampling dates.

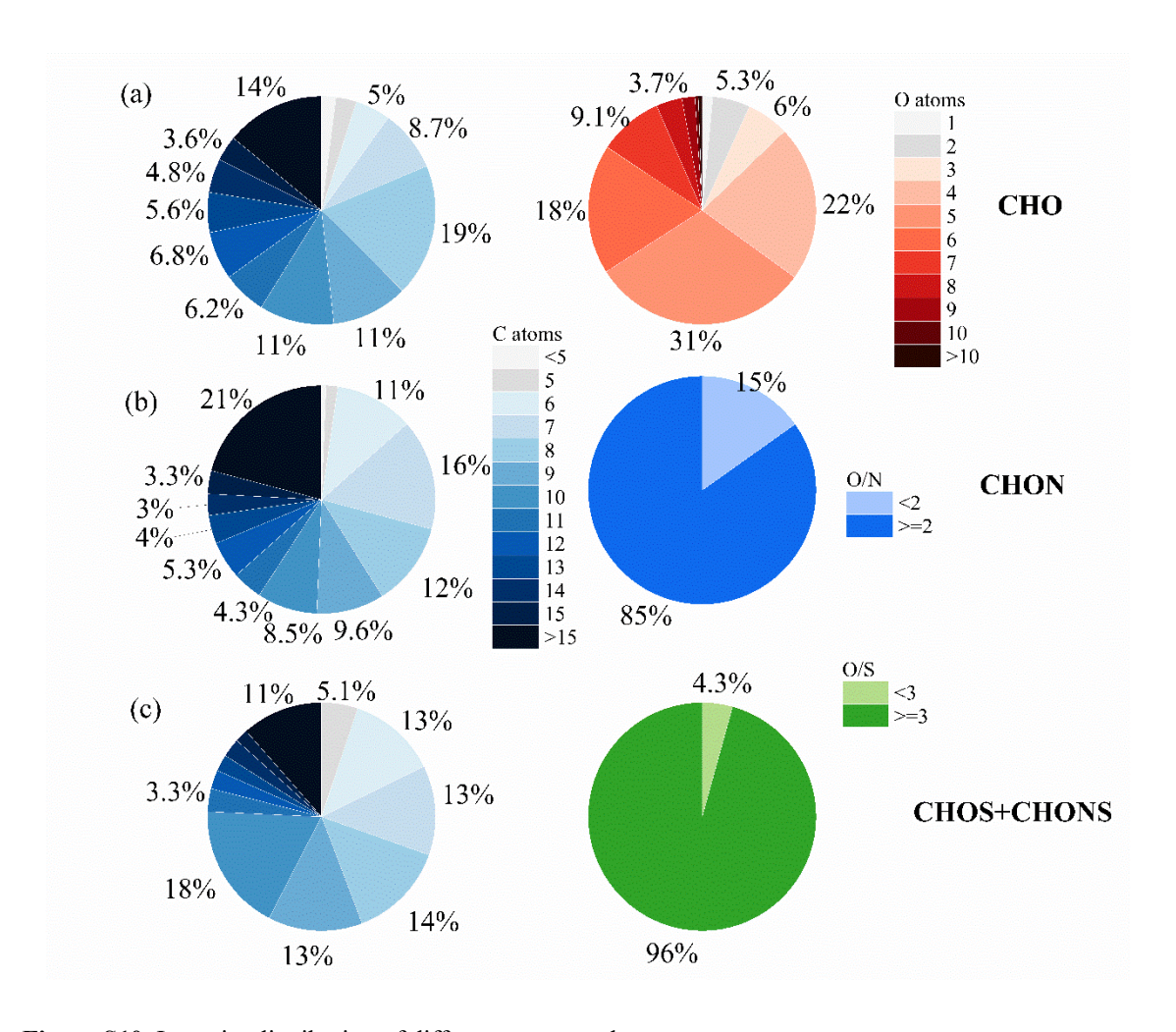


Figure S10. Intensity distribution of different compound groups

178

180

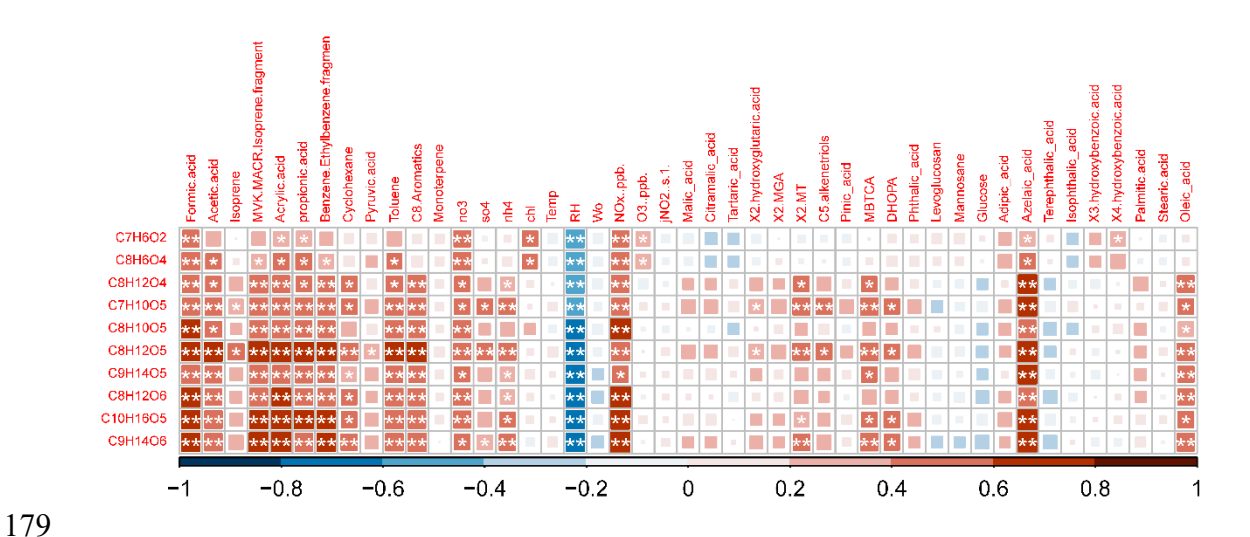


Figure S11. Correlations between the intensities of several highly abundant CHO compounds and selected chemical species.

Table S1. Sampling information for offline PM_{2.5} samples.

183

Sampling ID	Sampling	PM _{2.5}	Temp (°C)	RH (%)	OC (μg·m ⁻	EC (μg·m ⁻
	date	$(\mu g \cdot m^{-3})$	- , ,		3)	3)
HT01	2020/10/07	16.4	24.3	72	5.41	1.63
HT02	2020/10/08	16.8	25.0	68	5.05	1.60
HT03	2020/10/09	22.0	25.6	68	6.73	2.10
HT04	2020/10/10	13.8	26.7	76	4.92	1.97
HT05	2020/10/11	13.5	26.6	82	4.36	1.13
HT06	2020/10/12	14.5	25.9	77	5.99	2.56
HT07	2020/10/15	17.0	25.7	78	4.63	1.31
HT08	2020/10/16	16.0	24.6	77	4.25	1.26
HT09	2020/10/17	14.8	24.0	77	3.97	1.31
HT10	2020/10/18	18.3	23.4	70	2.56	1.27
HT11	2020/10/19	21.0	24.4	62	2.78	1.16
HT12	2020/10/20	16.0	25.6	61	2.87	0.96
HT13	2020/10/21	20.8	23.5	54	3.70	1.19
HT14	2020/10/22	23.2	23.5	70	5.45	1.04
HT15	2020/10/23	13.0	24.2	76	1.70	0.55
HT16	2020/10/24	11.4	24.0	81	1.67	0.60
HT17	2020/10/25	10.7	23.3	84	1.60	0.59
HT18	2020/10/27	19.7	23.9	84	2.11	1.19
HT19	2020/10/28	20.2	23.5	76	2.81	0.86
HT20	2020/10/29	12.5	23.2	72	2.08	0.76
HT21	2020/10/30	20.9	23.9	72	2.65	0.95
HT22	2020/10/31	26.7	23.5	67	3.57	1.45
HT23	2020/11/01	26.8	23.3	69	4.01	1.35
HT24	2020/11/02	16.6	24.2	60	2.15	0.83
HT25	2020/11/03	11.7	22.8	77	1.48	0.74
HT26	2020/11/04	34.8	26.1	59	5.20	2.05
HT27	2020/11/05	22.0	22.4	66	3.68	1.18
HT28	2020/11/06	16.4	21.7	67	2.20	0.71
HT29	2020/11/10	19.4	22.6	68	3.62	1.43
HT30	2020/11/11	21.3	22.0	80	2.55	1.03
HT31	2020/11/13	19.0	23.0	77	1.60	0.61

Table S2. Quantified compounds identified using TAG-EI-TOF-MS.

Compounds	Abbreviations	IS
Malic acid	MA	¹³ C-Pentaerythritol
Citramalic acid	CA	¹³ C-Pentaerythritol
Tartaric acids	TA	¹³ C-Pentaerythritol
2-hydroxyglutaric acid	2-HGA	¹³ C-Pentaerythritol
2-methylglyceric acid	2-MGA	¹³ C-Pentaerythritol
cis-2-methyl-1,3,4trihydroxy-1-butene		¹³ C-Pentaerythritol
3-methyl-2,3,4trihydroxy-1-butene	C5-alkenetriols	¹³ C-Pentaerythritol
trans-2-methy-1,3,4trihydroxy-1-butene		¹³ C-Pentaerythritol
2-methylthreitol	2-MTs	¹³ C-Pentaerythritol
2-methylerythritol	Z-WHS	¹³ C-Pentaerythritol
Pinic acid	PA	1-Dodecan-D25-ol
3-methyl-1,2,3butanetricarboxylic acid	MBTCA	¹³ C-Pentaerythritol
2,3-dihydroxy-4oxopentanoic acid	DHOPA	¹³ C-Pentaerythritol
Phthalic acid	PhA	D-phthalic acid
Terephthalic acid	TPA	D-phthalic acid
Isophthalic acid	IPA	D-Pentadecanol
Levoglucosan	Lev	¹³ C-Pentaerythritol
Mannosane	Man	¹³ C-Pentaerythritol
Glucose	Glu	¹³ C-Pentaerythritol
Adipic acid	AdiA	D-adipic acid
Azelaic acid	AzeA	D-Pentadecanol
3-hydroxybenzoic acid	3-HBA	1-Dodecan-d25-ol
4-hydroxybenzoic acid	4-HBA	1-Dodecan-d25-ol
Palmitic acid	PalA	1-Octadeca-d37-nol
Stearic acid	StA	Stearic-d35 acid
Oleic acid	OleA	Stearic-d35 acid
C20		Eicosane-d42
C21		Eicosane-d42
C22		Docosane-d46
C23		Docosane-d46
C24		Tetracosane-d50
C25		Tetracosane-d50
C26		Hexacosane-d54
C27		Hexacosane-d54
C28		Octacosane-d58
C29		Octacosane-d58
C30		Triacontane-d62
C31		Triacontane-d62
C32		Dotriacontane-d66
C33		Dotriacontane-d66
C34		Tetratriacontane-d70

 $\textbf{Table S3}. \ \text{Most intense compounds detected within wach compound group.} \\$

Formula	MW	DBE	AI_{mod}	VOC class	Structural	Possible name or Precursors		
CHO compounds								
Fatty acids (Sun et al.								
$C_6H_{10}O_1$	98.19	2	0.27	VOC	Lipids	2011)		
						Benzoic acid and		
$C_7H_6O_2$	122.17	5	0.67	IVOC	CRAMS	hydroxybenzaldehyde		
-						Trimethyl benzene		
$C_7H_{10}O_2$	126.20	3	0.33	IVOC	CRAMS	isomers (Mehra et al.,		
- /10 - 2		_	*****			2020)		
						Trimethyl benzene		
$C_7H_{10}O_4$	158.20	3	0.20	IVOC	CRAMS	isomers (Mehra et al.,		
, 10 1						2020)		
C ₈ H ₆ O ₄	166.19	6	0.67	IVOC	CRAMS	Phthalic acid		
'	172.24	2	0.17	IVOC	CDAMC	cis-Norpinic acid/		
$C_8H_{12}O_4$	172.24	3	0.17	IVOC	CRAMS	terpenylic acid		
C ₇ H ₁₀ O ₅	174.20	3	0.11	IVOC	HOC	Bicyclic hydroperoxide		
C ₈ H ₁₄ O ₄	174.25	2	0.00	IVOC	Protein	Suberic acid		
C ₇ H ₁₂ O ₅	176.22	2	0.00	IVOC	Carbohydrates	Monoterpenes		
C ₈ H ₆ O ₅	182.19	6	0.64	IVOC	CRAMS	Hydroxyphthalic acid		
						Trimethyl benzene		
$C_8H_{10}O_5$	186.22	4	0.27	IVOC	CRAMS	isomers/ monoterpenes		
C ₉ H ₁₄ O ₄	186.27	3	0.14	IVOC	Protein	Pinic acid		
	100.22	2	0.00	ILLOG	CD 414G	Monoterpene /		
$C_8H_{12}O_5$	188.23	3	0.09	IVOC	CRAMS	hydroxyterpenylic acid		
G.H. O	100.20	2	0.00	ILLOG	ъ	Azelaic acid /		
$C_9H_{16}O_4$	188.29	2	0.00	IVOC	Protein	monoterpene		
C.H. O	100.25	2	0.00	ILLOC	D	Diaterpenylic acid/		
$C_8H_{14}O_5$	190.25	2	0.00	IVOC	Protein	monoterpene		
	200.25	4	0.22	IVOC	CDAMC	Aromatics (Molteni et		
$C_9H_{12}O_5$	200.25	4	0.23	IVOC	CRAMS	al., 2018)		
	Trimethyl be							
$C_8H_{10}O_6$	202.22	4	0.20	SVOC	HOC	isomers/ isoprene		
						(Nguyen et al., 2011)		
C ₉ H ₁₄ O ₅	202.27	3	0.08	IVOC	Protein	Monoterpene		
	204.22			CLIOC		Monoterpene/		
$C_8H_{12}O_6$	204.23	3	0.00	SVOC	HOC	Trimethylbenzene		
C ₁₀ H ₁₄ O ₅	214.29	4	0.20	IVOC	CRAMS	Monoterpene		
C ₁₀ H ₁₆ O ₅	216.30	3	0.07	IVOC	Protein	Monoterpene		
'						Monoterpene/		
$C_9H_{14}O_6$	218.27	3	0.00	SVOC	Protein	Trimethylbenzene		
	222.22		0.40	HIGG	CD 13.60	Monoterpene/biomass		
$C_{12}H_{14}O_4$	222.32	6	0.40	IVOC	CRAMS	burning		
$C_{10}H_{14}O_6$	230.29	4	0.14	SVOC	CRAMS	Monoterpene		
$C_{11}H_{18}O_5$	230.34	3	0.06	SVOC	Protein	Monoterpene		
$C_{10}H_{16}O_{6}$	232.30	3	0.00	SVOC	Protein	Monoterpene		
$C_{12}H_{18}O_5$	242.35	4	0.16	SVOC	CRAMS	Monoterpene		
$\frac{C_{12}H_{16}O_{5}}{C_{11}H_{16}O_{6}}$	244.32	4	0.13	SVOC	CRAMS	Biogenic		
$C_{12}H_{20}O_5$	244.37	3	0.05	SVOC	Protein	Biogenic		
$\frac{C_{12}H_{20}O_5}{C_{13}H_{20}O_5}$	256.39	4	0.14	SVOC	Protein	β-Caryophyllene		
213112003	250.57	т		N compour		p caryophynene		
C ₆ H ₅ NO ₃	139.15	5	0.86	IVOC	CRAMS	Nitrophenol/catechol		
C611511O3	137.13	5	0.00	1100	CIVAIND	14110phenol/catechol		

$C_5H_4N_2O_3$	140.13	5	1.67	IVOC	CRAMS	Methylglyoxal
3 . 2 3						+Ammonium Sulfate
C ₇ H ₇ NO ₃	153.19	5	0.67	IVOC	CRAMS	Nitrocresol
C ₆ H ₅ NO ₄	155.15	5	0.83	IVOC	CRAMS	4-Nitrocatechol
$C_8H_6N_2O_2$	162.20	7	1.00	SVOC	CRAMS	3-Nitroindole
$C_7H_4N_2O_3$	164.17	7	1.29	SVOC	Condensed	\
	1.5.00		^ -2	*****	Aromatics	
$C_8H_7NO_3$	165.20	6	0.73	IVOC	CRAMS	Nitroacetophenone or
						methyl- nitrobenzaldehyde
C ₈ H ₉ NO ₃	167.22	5	0.55	IVOC	CRAMS	Dimethyl-nitrophenol
C ₇ H ₇ NO ₄	169.18	5	0.63	SVOC	CRAMS	2-Methyl-4-
C/11/1104	107.10	3	0.03	5,000	CICAIVIS	nitroresorcinol
C ₇ H ₅ NO ₅	183.17	6	0.86	SVOC	HOC	2-Methyl-5-
0/11/11/05	103.17	Ü	0.00	5,00	1100	nitrobenzoic acid
C ₉ H ₁₇ NO ₃	187.30	2	0.00	SVOC	Protein	Biomass burning
$C_{10}H_7NO_3$	189.24	8	0.80	SVOC	CRAMS	2-Nitro-1-naphthol
C ₉ H ₇ NO ₄	193.22	7	0.75	SVOC	CRAMS	Biomass burning
C ₈ H ₇ NO ₅	197.20	6	0.67	SVOC	CRAMS	Methyl-hydroxy-
						nitrobenzoate
C ₈ H ₉ NO ₅	199.22	5	0.44	SVOC	CRAMS	Dimethoxy-nitrophenol
$C_7H_4N_2O_7$	228.17	7	1.67	LVOC	Others	Toluene/ 3,5-
						dinitrosalicylic acid
$C_6H_3N_3O_7$	229.15	7	0.00	LVOC	Others	Picric acid
$C_{23}H_{17}N_3O_2$	367.56	17	0.76	ELVOC	Unsaturated	\
					Hydrocarbons	
C ₂₃ H ₄₉ NO ₄	403.80	0	0.00	LVOC	Others	\
$C_{27}H_{17}N_5O_{16}$	667.64	22	0.82	ULVOC	Condensed	\
			TIOC - C	HONG	Aromatics	
	210.25			HONS com		C 1. f 1. t'1
$\frac{C_6H_{10}O_6S_1}{C_1H_1O_1S_1}$	210.25	2	0	SVOC SVOC	Others Others	Green leaf volatiles
$C_6H_{12}O_6S_1$	212.26	1	U	SVOC	Otners	Monoterpene/ olefinic acid
$C_5H_{10}O_7S_1$	214.23	1	0	LVOC	Others	Isoprene/ olefinic acid
$C_7H_{12}O_6S_1$	224.28	2	0	SVOC	Carbohydrates	Monoterpene
$C_6H_{10}O_7S_1$	226.25	2	0	LVOC	Others	Isoprene/ green leaf volatiles
$C_7H_{14}O_6S_1$	226.30	1	0	SVOC	Carbohydrates	Olefinic acid
$C_6H_{12}O_7S_1$	228.26	1	0	LVOC	Others	Isoprene
$C_7H_{12}O_7S_1$	240.28	2	0	LVOC	Others	Isoprene
$C_6H_{10}O_8S_1$	242.25	2	0	LVOC	Others	\
C ₉ H ₁₆ O ₆ S ₁	252.35	2	0	SVOC	Protein	Monoterpene
C ₈ H ₁₄ O ₇ S ₁	254.32	2	0	LVOC	Carbohydrates	Monoterpene
C ₇ H ₁₂ O ₈ S ₁	256.28	2	0	LVOC	Others	Isoprene
$C_8H_{12}O_8S_1$	268.30	3	0	LVOC	НОС	Monoterpene
$C_{10}H_{16}O_{7}S_{1}$	280.37	3	0	LVOC	Carbohydrates	Monoterpene
C ₉ H ₁₄ O ₈ S ₁	282.33	3	0	LVOC	Carbohydrates	Monoterpene
$C_{10}H_{18}O_7S_1$	282.38	2	0	LVOC	Carbohydrates	Monoterpene
$C_8H_{12}O_9S_1$	284.30	3	0	LVOC	Others	\
C ₉ H ₁₆ O ₈ S ₁	284.35	2	0	LVOC	Carbohydrates	Monoterpene
$C_{10}H_{17}O_7N_1S_1$	295.38	3	0	ELVOC	Carbohydrates	Monoterpene
$C_{10}H_{16}O_8S_1$	296.37	3	0	LVOC	Carbohydrates	Monoterpene

Table S4. Intensity-weighted molecular characteristics of organic compounds associated with NMF-derived OA factors

	C-OA _{NMF}	Iso-SOA _{NMF}	BB-OA _{NMF}	gas- pSOA _{NMF}	SIA-OA _{NMF}
MW	216	213	217	221	214
C	8.91	9.44	10.00	9.25	9.76
Н	12.75	13.38	12.92	12.78	13.76
O	5.25	5.02	4.81	5.42	4.83
N	0.22	0.11	0.33	0.20	0.17
S	0.28	0.12	0.07	0.23	0.10
H/C	1.44	1.42	1.28	1.38	1.40
O/C	0.63	0.59	0.52	0.63	0.56
N/C	0.03	0.01	0.04	0.03	0.02
S/C	0.04	0.01	0.01	0.03	0.01
O/N	0.88	0.30	1.09	0.71	0.40
O/S	1.84	0.75	0.43	1.59	0.56
N/S	0.09	0.04	0.03	0.04	0.03
DBE	3.64	3.81	4.71	3.96	3.97
DBE/C	0.41	0.42	0.49	0.44	0.43
nO_{eff}	3.97	4.43	3.94	4.34	4.18
AI_{mod}	0.20	0.22	0.34	0.24	0.24
Xc	1.40	1.28	1.70	1.46	1.40
$LogC^*$	1.42	2.12	1.90	1.39	2.09
		Compounds	s classes		
DBE=0	0.68	1.76	0.30	0.65	1.2
DBE=1	5.8	4.6	4.0	4.8	3.9
DBE=2	19	17	13	18	14
DBE=3	29	28	22	25	22
DBE >= 4	45	49	61	51	58
Condensed	3.7	3.3	5.6	3.0	3.1
Aromatics					
CRAMS	36	34	43	36	38
Lipids-like	4.7	7.4	10.6	6.1	9.1
Protein-like	18	25	20	21	19
HOC	12	11	10	12	13
Carbohydrates-	12	5	4	8	2
like					
Unsaturated	0.88	1.25	0.72	0.56	2.7
Hydrocarbons					
Others	13	14	5	13	13

References

- Ditto, J. C., Barnes, E. B., Khare, P., Takeuchi, M., Joo, T., Bui, A. A. T., Lee-Taylor, J., Eris, G., Chen, Y., Aumont, B., Jimenez, J. L., Ng, N. L., Griffin, R. J., and Gentner, D. R.: An omnipresent diversity and variability in the chemical composition of atmospheric functionalized organic aerosol, Communications Chemistry, 1, 75, doi:10.1038/s42004-018-0074-3, 2018.
- Huo, Y., Yao, D., and Guo, H.: Differences in aerosol chemistry at a regional background site in Hong Kong before and during the COVID-19 pandemic, Sci Total Environ, 926, 171990, doi:10.1016/j.scitotenv.2024.171990, 2024a.
- Huo, Y., Lyu, X., Yao, D., Zhou, B., Yuan, Q., Lee, S. c., and Guo, H.: Exploring the Formation of High Levels of Hydroxyl Dicarboxylic Acids at an Urban Background Site in South China, Journal of Geophysical Research: Atmospheres, 129, e2023JD040096, doi:10.1029/2023jd040096, 2024b. Koch, B. P. and Dittmar, T.: From mass to structure: an aromaticity index for high-resolution mass data of
- natural organic matter, Rapid Communications in Mass Spectrometry, 20, 926–932, doi:10.1002/rcm.2386, 2006.
- Li, Y., Pöschl, U., and Shiraiwa, M.: Molecular corridors and parameterizations of volatility in the chemical evolution of organic aerosols, Atmospheric Chemistry and Physics, 16, 3327-3344, doi:10.5194/acp-16-3327-2016, 2016.
- Lyu, X., Guo, H., Yao, D., Lu, H., Huo, Y., Xu, W., Kreisberg, N., Goldstein, A. H., Jayne, J., Worsnop, D., Tan, Y., Lee, S. C., and Wang, T.: In Situ Measurements of Molecular Markers Facilitate Understanding of Dynamic Sources of Atmospheric Organic Aerosols, Environ Sci Technol, 54, 11058-11069, doi:10.1021/acs.est.0c02277, 2020.
- Mehra, A., Wang, Y., Krechmer, J. E., Lambe, A., Majluf, F., Morris, M. A., Priestley, M., Bannan, T. J., Bryant, D. J., Pereira, K. L., Hamilton, J. F., Rickard, A. R., Newland, M. J., Stark, H., Croteau, P., Jayne, J. T., Worsnop, D. R., Canagaratna, M. R., Wang, L., and Coe, H.: Evaluation of the chemical composition of gas- and particle-phase products of aromatic oxidation, Atmospheric Chemistry and Physics, 20, 9783-9803, doi:10.5194/acp-20-9783-2020, 2020.
- Molteni, U., Bianchi, F., Klein, F., El Haddad, I., Frege, C., Rossi, M. J., Dommen, J., and Baltensperger, U.: Formation of highly oxygenated organic molecules from aromatic compounds, Atmospheric Chemistry and Physics, 18, 1909-1921, doi:10.5194/acp-18-1909-2018, 2018.
- Nguyen, T. B., Roach, P. J., Laskin, J., Laskin, A., and Nizkorodov, S. A.: Effect of humidity on the composition of isoprene photooxidation secondary organic aerosol, Atmospheric Chemistry and Physics, 11, 6931-6944, doi:10.5194/acp-11-6931-2011, 2011.
- Nie, W., Yan, C., Huang, D. D., Wang, Z., Liu, Y., Qiao, X., Guo, Y., Tian, L., Zheng, P., Xu, Z., Li, Y., Xu, Z., Qi, X., Sun, P., Wang, J., Zheng, F., Li, X., Yin, R., Dallenbach, K. R., Bianchi, F., Petäjä, T., Zhang, Y., Wang, M., Schervish, M., Wang, S., Qiao, L., Wang, Q., Zhou, M., Wang, H., Yu, C., Yao, D., Guo, H., Ye, P., Lee, S., Li, Y. J., Liu, Y., Chi, X., Kerminen, V.-M., Ehn, M., Donahue, N. M., Wang, T., Huang, C., Kulmala, M., Worsnop, D., Jiang, J., and Ding, A.: Secondary organic aerosol formed by condensing anthropogenic vapours over China's megacities, Nature Geoscience, 15, 255-261, doi:10.1038/s41561-022-00922-5, 2022.
- Sun, Y. L., Zhang, Q., Schwab, J. J., Demerjian, K. L., Chen, W. N., Bae, M. S., Hung, H. M., Hogrefe, O., Frank, B., Rattigan, O. V., and Lin, Y. C.: Characterization of the sources and processes of organic and inorganic aerosols in New York city with a high-resolution time-of-flight aerosol mass apectrometer, Atmospheric Chemistry and Physics, 11, 1581-1602, doi:10.5194/acp-11-1581-2011, 2011.
- Thoma, M., Bachmeier, F., Gottwald, F. L., Simon, M., and Vogel, A. L.: Mass spectrometry-based Aerosolomics: a new approach to resolve sources, composition, and partitioning of secondary organic aerosol, Atmospheric Measurement Techniques, 15, 7137-7154, doi:10.5194/amt-15-7137-2022, 2022.
- Wang, X., Hayeck, N., Brüggemann, M., Yao, L., Chen, H., Zhang, C., Emmelin, C., Chen, J., George, C., and Wang, L.: Chemical Characteristics of Organic Aerosols in Shanghai: A Study by Ultrahigh-Performance Liquid Chromatography Coupled With Orbitrap Mass Spectrometry, J. Geophys. Res. Atmos.,
- Performance Liquid Chromatography Coupled With Orbitrap Mass Spectrometry, J. Geophys. Res. Atmos. 122, 11703–11722, doi:10.1002/2017jd026930, 2017.
- Yao, D., Guo, H., Lyu, X., Lu, H., and Huo, Y.: Secondary organic aerosol formation at an urban background site on the coastline of South China: Precursors and aging processes, Environmental Pollution, 309, 119778, doi:10.1016/j.envpol.2022.119778, 2022.

Yuan, Q., Zhang, Z., Chen, Y., Hui, L., Wang, M., Xia, M., Zou, Z., Wei, W., Ho, K. F., Wang, Z., Lai, S., Zhang, Y., Wang, T., and Lee, S.: Origin and transformation of volatile organic compounds at a regional background site in Hong Kong: Varied photochemical processes from different source regions, Sci Total Environ, 908, 168316, doi:10.1016/j.scitotenv.2023.168316, 2024.

Zhang, M., Cai, D., Lin, J., Liu, Z., Li, M., Wang, Y., and Chen, J.: Molecular characterization of atmospheric organic aerosols in typical megacities in China, npj Climate and Atmospheric Science, 7, 230, doi:10.1038/s41612-024-00784-1, 2024.

Zhang, Q., Jimenez, J. L., Canagaratna, M. R., Ulbrich, I. M., Ng, N. L., Worsnop, D. R., and Sun, Y.: Understanding atmospheric organic aerosols via factor analysis of aerosol mass spectrometry: a review, Anal Bioanal Chem, 401, 3045-3067, doi:10.1007/s00216-011-5355-y, 2011.